ELSEVIER

Biochimica et Biophysica Acta 1456 (2000) 56–66

BIOCHIMICA ET BIOPHYSICA ACTA
BBA

www.elsevier.com/locate/bba

The reactions of hydrogen peroxide with bovine cytochrome *c* oxidase

Susanne Jünemann [a], Peter Heathcote [b], Peter R. Rich [a,*]

[a] *The Glynn Laboratory of Bioenergetics, Department of Biology, University College London, Gower Street, London WC1E 6BT, UK*
[b] *School of Biological Sciences, Queen Mary and Westfield College, Mile End Road, LondonE1 4NS, UK*

Received 3 May 1999; received in revised form 21 September 1999; accepted 8 November 1999

Abstract

Oxidised cytochrome *c* oxidase is known to react with two molecules of hydrogen peroxide to form consecutively 607 nm '**P**eroxy' and 580-nm '**F**erryl' species. These are widely used as model compounds for the equivalent **P** and **F** intermediates of the catalytic cycle. However, kinetic analysis of the reaction with H_2O_2 in the pH range 6.0–9.0 reveals a more complex situation. In particular, as the pH is lowered, a 580-nm compound can be formed by reaction with a single H_2O_2. This species, termed $\mathbf{F}^{\bullet}$, is spectrally similar, but not identical, to **F**. The reactions are equivalent to those previously reported for the *bo* type quinol oxidase from *Escherichia coli* (T. Brittain, R.H. Little, C. Greenwood, N.J. Watmough, FEBS Lett. 399 (1996) 21–25) where it was proposed that $\mathbf{F}^{\bullet}$ is produced directly from **P**. However, in the bovine oxidase $\mathbf{F}^{\bullet}$ does not appear in samples of the 607-nm form, $\mathbf{P}_M$, produced by CO/O_2 treatment, even at low pH, although this form is shown to be identical to the H_2O_2-derived **P** state, $\mathbf{P}_H$, on the basis of spectral characteristics and kinetics of reaction with H_2O_2. Furthermore, lowering the pH of a sample of $\mathbf{P}_M$ or $\mathbf{P}_H$ generated at high pH results in $\mathbf{F}^{\bullet}$ formation only on a minutes time scale. It is concluded that **P** and $\mathbf{F}^{\bullet}$ are not in a rapid, pH-dependent equilibrium, but instead are formed by distinct pathways and cannot interconvert in a simple manner, and that the crucial difference between them lies in their patterns of protonation.

Keywords: Cytochrome *c* oxidase; Hydrogen peroxide; P-state; F-state; EPR

1. Introduction

The catalytic mechanism of oxygen reduction by cytochrome *c* oxidase is thought to include 'peroxy' (**P**) and 'ferryl' (**F**) intermediates (c.f. [1]). These species were first described in reversed electron transfer studies using coupled mitochondria [2,3], and have since been observed in the forward reaction of fully reduced cytochrome *c* oxidase [4,5] and other haem-copper oxidases [6,7] with oxygen. In the visible region **P** and **F** are characterised by distinct peaks at 607 nm and near 580 nm, respectively, but in the Soret region both species exhibit a similar red-shift relative to the oxidised state [8]. Overall, the redox states of **P** and **F** differ from the oxidised enzyme (**O**) by 2 and 3 reducing equivalents, respectively [9]. Whereas **F** is recognised to be an Fe(IV)=O Cu_B(II) ferryl compound, the structure of **P** (formally a ferric-peroxy adduct) has been controversial, particularly on the point of whether the O–O bond is intact. Recent MCD, resonance Raman and other data sug-

* Corresponding author. Fax: +44-171-380-7746; E-mail: prr@ucl.ac.uk

0005-2728/00/$ – see front matter
PII: S0005-2728(99)00105-X

gest that both intermediates may be ferryl species [10–14].

Species related to **P** and **F** can be formed by alternative means. At high pH, incubation of oxidised enzyme with CO and oxygen results in a 607 nm compound [15,16], presumably by a two electron reduction by CO, followed by reaction of the mixed-valence product with oxygen. This has been termed $\mathbf{P}_M$ to distinguish it from the **P** state transiently formed in the oxygen reaction of fully reduced enzyme ($\mathbf{P}_R$) where the binuclear centre contains an additional electron on Cu_B [4].

Oxidised enzyme can also react with H_2O_2 to produce 607- and 580-nm compounds. The extent and rate of reaction, and the ratio of the forms, depend on pH and H_2O_2 concentration [17–19]. Briefly, low pH will yield largely, or even exclusively, the 580-nm species whilst higher pH and micromolar H_2O_2 levels will favour accumulation of a 607-nm compound, here called $\mathbf{P}_H$.

It has been shown [20] that the reaction of oxidised cytochrome *bo* from *E. coli* with H_2O_2 proceeds via the $\mathbf{P}_H$ state to two spectrally identical ferryl compounds, termed **F** and $\mathbf{F}^\bullet$. **F** is formed from $\mathbf{P}_H$ by reaction with a second H_2O_2 molecule, whereas $\mathbf{F}^\bullet$ is thought to be generated from $\mathbf{P}_H$ in a unimolecular reaction, presumably by taking an electron from a site within the protein, possibly by oxidation of Cu(II) to Cu(III) or by the formation of a free radical from an amino acid side chain or the haem group [13,20]. There is evidence that oxidised bovine enzyme may also react with H_2O_2 by two pathways to form **F** and $\mathbf{F}^\bullet$ (cf. [9,19]), but conclusive data are as yet lacking. Two radical EPR signals were observed following the incubation of cytochrome *c* oxidase with H_2O_2 [19], although at low occupancy (less than 0.1 spin per enzyme) and with maximum intensity for the dominant signal under conditions where, by inference from the data on cytochrome *bo* from *E. coli* [20], formation of **F** rather than $\mathbf{F}^\bullet$ is expected. However, in a more recent study of *Paracoccus denitrificans* cytochrome *c* oxidase [21] only one radical species, attributed to a tyrosine, was found on reaction with H_2O_2.

In this paper we investigate the possible multiplicity of 607- and 580-nm forms in bovine cytochrome *c* oxidase, and their relation to each other.

2. Materials and methods

2.1. Preparation of bovine heart oxidase

Cytochrome *c* oxidase was prepared by a procedure [22] which yields 'fast' enzyme with monophasic cyanide binding kinetics and a characteristic Soret maximum at 424 nm. It was quantitated optically from the dithionite-reduced *minus* oxidised difference spectrum using an extinction coefficient of $\Delta\varepsilon_{606-621\,nm} = 25.7\ mM^{-1}\,cm^{-1}$ [8].

2.2. Optical spectroscopy

Optical spectra and multiwavelength kinetics were monitored at room temperature in the same sample using a single-beam instrument built in house.

2.3. Calibration of H_2O_2 solutions

The H_2O_2 stock was a 30% (w/v) stabilised solution, i.e. equivalent to 8.8 M H_2O_2, which was stored at 4°C. Dilutions to between 500 and 5 mM were prepared in double-distilled water and calibrated optically using an extinction coefficient at 240 nm of $40\ M^{-1}\,cm^{-1}$ [23]. Values agreed with concentrations determined by measurement of the oxygen evolved when the solution was added to 50 mM potassium phosphate pH 7.5 containing 10^4 U/ml catalase in a Clark-type electrode. Diluted solutions were kept on ice and used within 4 h.

2.4. Electron paramagnetic resonance spectroscopy

Continuous-wave EPR spectra were recorded on a Jeol RE1X spectrometer fitted with an Oxford Instruments cryostat. Conditions of measurement were as indicated in the figure legends. Spin intensities were quantitated by double-integration and calibrated against a sample of known concentration of photo-oxidised P700 in photosystem I particles from spinach, prepared using Triton X-100 as described previously [24]. The concentration of P700 was determined optically from an ascorbate-reduced *minus* ferricyanide-oxidised difference spectrum using an extinction coefficient of 64 $mM^{-1}\ cm^{-1}$ at 703 nm. $P700^+$ was generated by illuminating the sample

in the EPR tube for 60 s and freezing in liquid nitrogen under illumination.

2.5. Kinetic simulations

In order to account for intermediates during a sequential reaction, the kinetics of reaction of H_2O_2 with cytochrome *c* oxidase were analysed by computer simulation using KINSIM software [25,26]. In order to simulate data in the visible region, a matrix of extinction coefficients for $\mathbf{P}_H$ and **F** relative to oxidised enzyme is required (Table 1) which was derived from values given in [8]. Since the peak positions and extinction coefficients of both compounds show only slight pH-dependent variations, only a single set of extinction coefficients was used for all pH values.

3. Results

3.1. Kinetics and pH dependency of the interaction of H_2O_2 with cytochrome c oxidase

As shown in Fig. 1A, the reaction of cytochrome *c* oxidase with H_2O_2 gave varying amounts of 607- and 580-nm species depending on pH and H_2O_2 concentration (c.f. [19]). At pH 6.5, reaction of H_2O_2 yielded almost entirely a 580-nm compound, regardless of H_2O_2 concentration. In contrast, at pH 8.5, low H_2O_2 levels resulted in predominantly the 607-nm form $\mathbf{P}_H$ with contaminations by 580-nm species too small to perturb the shape and position of the $\mathbf{P}_H$ β-peak at 568–570 nm, whereas with millimolar H_2O_2 the product was purely a 580-nm compound.

Kinetics were measured over a concentration range of 10–5000 μM H_2O_2, and in the pH range 6.0–9.0. As the reaction may be coupled to release of superoxide [27], superoxide dismutase was included in all assays. Indeed, the absence of superoxide dismutase led to spectral distortions in the Soret region and the appearance of an additional kinetic phase due to accelerated decay of the 580-nm species (not shown). This effect was more pronounced at low pH (<7.0) and/or higher (>250 μM) H_2O_2 concentrations.

It has previously been reported that incubation of oxidised enzyme at low pH affects the extent and number of kinetic phases [18]. However, this was seen following extended (hours) preincubation at low pH and was hence likely to arise from accumulation of 'slow' enzyme. In the present experiments, the enzyme was exposed to low pH for no more than 10 min during the course of the reaction with H_2O_2, so that conversion of unreacted 'fast' oxidase to the 'slow' form was negligible. This was confirmed by the unchanged extent of reaction over the pH range studied and by the absence of any additional kinetic phases attributable to the 'slow' form.

As the Soret band positions and extinction coefficients of the 607- and 580-nm species are very similar

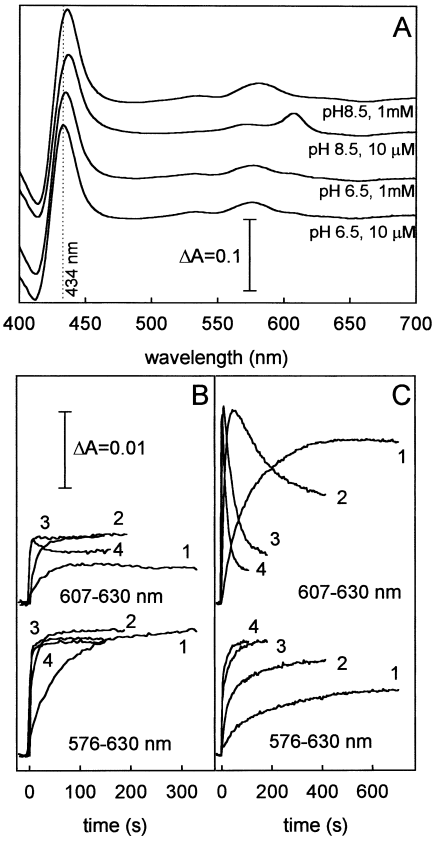

Fig. 1. pH and H_2O_2 concentration dependency of reaction of H_2O_2 with oxidised cytochrome *c* oxidase. 'Fast' bovine heart cytochrome *c* oxidase (3.5 μM) was suspended in 0.1 M potassium phosphate buffer containing 0.05% (w/v) lauryl maltoside and 80 U/ml superoxide dismutase. Difference spectra at equilibrium versus oxidised cytochrome *c* oxidase are shown in A. The lower panel shows kinetic experiments at pH 6.5 (B) and 8.5 (C). At $t=0$ s, H_2O_2 was added to the following final concentrations: (1) 10 μM, (2) 100 μM, (3) 500 μM, and (4) 1000 μM. Monitoring wavelengths are as indicated. Note that B and C have the same ΔA scale, but different time scales.

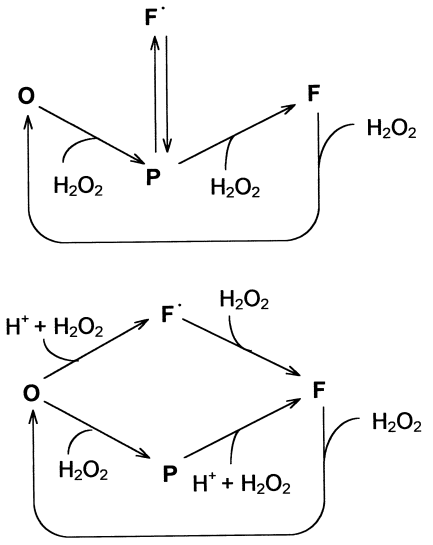

Fig. 2. Mechanistic models for the reaction of oxidised cytochrome *c* oxidase with H_2O_2. Top: Scheme 1. Bottom: Scheme 2.

(see Fig. 1A) progress curves recorded in the Soret region reflect largely the interaction of the first H_2O_2 molecule with **O**, and are only little affected by further reaction steps. Hence, we focused on kinetic changes in the visible region where multiphasic kinetics were observed at 607 *minus* 630 nm (representing predominantly $\mathbf{P}_H$) and at 576 *minus* 630 nm (representing mostly the 580-nm species). Typical kinetic data for pH 6.5 and 8.5 are shown in Fig. 1B and C, respectively. At pH 8.5, transient formation of the 607 nm species occurs at H_2O_2-dependent rates, followed by a decay that is roughly concurrent with formation of the 580-nm form and is also H_2O_2 concentration-dependent. In contrast, at pH 6.5, much less 607-nm compound is observed, and instead formation of the 580-nm species predominates, again at an H_2O_2-dependent rate.

The experimental traces could be simulated with two types of model (Fig. 2). In Scheme 1 of Fig. 2, reaction with the first H_2O_2 produces $\mathbf{P}_H$ which then reacts by multiple pathways to yield two 580-nm compounds, $\mathbf{F}^\bullet$ and **F**. In particular, $\mathbf{F}^\bullet$ arises from $\mathbf{P}_H$ in a spontaneous equilibrium reaction. This mechanism is based on that previously described for cytochrome *bo* from *E. coli* [20], but omitting back reactions for the H_2O_2-dependent steps $\mathbf{O} \rightarrow \mathbf{P}_H$ and $\mathbf{P}_H \rightarrow \mathbf{F}$, and incorporating instead the reaction of **F** with a further molecule of H_2O_2 to regenerate the oxidised state [27]. This change did not significantly affect estimations of forward rate constants. In the mechanism of Scheme 2 of Fig. 2, $\mathbf{P}_H$ and $\mathbf{F}^\bullet$ are not directly related, but are alternative products of reaction of **O** with one H_2O_2 molecule, with $\mathbf{F}^\bullet$ formation favoured as the pH is lowered. A second H_2O_2 converts both $\mathbf{P}_H$ and $\mathbf{F}^\bullet$ to **F**. Other models, such as a linear two-step reaction from $\mathbf{P}_H$ to **F** via $\mathbf{F}^\bullet$ were also tested, but did not fit the data satisfactorily.

Using the mechanism of Scheme 2 (Fig. 2), a complete set of rate constants for the pH range studied was obtained, and values at pH 6 and 8 are summarised in Table 2. However, in order to allow comparison with data reported for the *bo*-type quinol oxidase from *E. coli* [20], the table also includes values obtained by kinetic analysis using Scheme 1 in Fig. 2.

3.2. Spectral characteristics of *F* and *F* •

Since the data of Fig. 1 and the deduced schemes of Fig. 2 imply that reaction of cytochrome *c* oxidase with H_2O_2 can yield two distinct 580-nm compounds, **F** and $\mathbf{F}^\bullet$, the question arises as to whether these show any spectral differences. Some indication of such differences may be seen in the spectra in Fig. 1A, where the 434-nm Soret peak position of the 580-nm compound produced at pH 6.5 and 10 μM

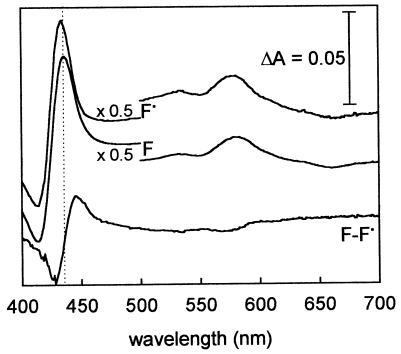

Fig. 3. A comparison of optical spectra of the F and $F^\bullet$ species. 'Fast' bovine heart cytochrome *c* oxidase (3.5 μM) was suspended in 0.1 M potassium phosphate buffer containing 0.05% (w/v) lauryl maltoside and 80 U/ml superoxide dismutase. **F** was generated with 1 mM H_2O_2 at pH 6.5 and $\mathbf{F}^\bullet$ with 10 μM H_2O_2 at pH 6.5, as in Fig. 1. Their difference spectra versus the oxidised enzyme were normalised so that both had a Soret band ΔA (peak to trough) of 1.0, and were then subtracted to obtain the **F** *minus* $\mathbf{F}^\bullet$ difference spectrum.

H_2O_2 and assumed to be primarily $\mathbf{F}^{\bullet}$ is consistently at a lower wavelength than the 435–436 nm Soret band of the 580-nm **F** species formed with 1mM H_2O_2 at pH 6.5 and at pH 8.5. This can be seen more clearly in Fig. 3 where difference spectra versus the oxidised enzyme of **F** (generated with 1 mM H_2O_2 at pH 6.5) and $\mathbf{F}^{\bullet}$ (generated with 10 μM H_2O_2 at pH 6.5) are plotted, together with the difference between them which highlights the shift in Soret band position. This shift persisted in samples containing potassium ferricyanide, making it unlikely that it was caused by partial reduction. Differences between the spectra in the visible region were less clear, but the absence of any peak in the 604–607-nm region also indicated that the Soret band difference did not arise from partial reduction.

3.3. Comparison of the *P*-type compounds generated with H_2O_2 and CO/O_2

Although $\mathbf{P}_M$, the 607 nm compound generated by the CO/O_2 method, appears to be spectrally identical to $\mathbf{P}_H$ (c.f. [19]), their equivalence has not been established definitively. In order to compare the two species further, we examined the effects of pH on $\mathbf{P}_M$ and the kinetics of its reaction with H_2O_2.

In the experiment of Fig. 4, $\mathbf{P}_M$ was generated by bubbling oxidised cytochrome *c* oxidase with carbon monoxide under aerobic conditions. The extent of $\mathbf{P}_M$ formation was strongly pH dependent with an apparent p*K* of 7.25 and an observed n value of 2 (Fig. 4A,B), reaching essentially quantitative conversion to $\mathbf{P}_M$ at pH 9.0. However, under anaerobic conditions the CO-bound mixed-valence state was formed quantitatively down to pH 6 [28]. Mixing with oxygen then quantitatively converted the mixed valence form solely to the 607 nm $\mathbf{P}_M$ which subsequently decayed to a degree which increased as the pH was lowered (not shown). Hence, the extent of $\mathbf{P}_M$ formation in Fig. 4 represents a steady state caused by the balance of rate of formation with the rate of reaction with a further CO to regenerate the oxidised state. The pH dependency of the steady-state occupancy level is due mostly to an accelerated reaction of $\mathbf{P}_M$ with CO (at 1 mM CO pseudo-first-order rate constants were 0.00065 and 0.015 s^{-1} at pH 9 and 6, respectively). At the same time, the pseudo-first-order rate constant of $\mathbf{P}_M$ formation decreases as the pH is lowered (0.0065 and 0.0015 s^{-1} at pH 9 and 6, respectively), although to a lesser extent than those of the onward reaction.

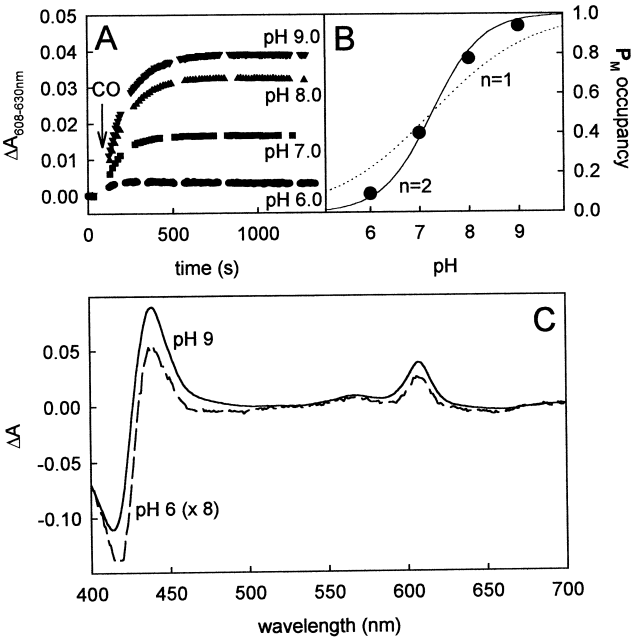

Fig. 4. Formation of $\mathbf{P}_M$ by aerobic incubation of oxidised cytochrome *c* oxidase with carbon monoxide. 3.5 μM cytochrome *c* oxidase were suspended in 0.1 M potassium phosphate buffer at various pH values and containing 0.05% (w/v) lauryl maltoside. Formation of $\mathbf{P}_M$ was initiated by slowly bubbling CO through the samples for 30 s under aerobic conditions. (A) formation of $\mathbf{P}_M$ monitored at 607 *minus* 630 nm. (B) Maximum extent of $\mathbf{P}_M$ formation versus pH. For comparison, experimental data are overlaid with curves calculated with the Henderson–Hasselbach equation for a site involving 1 (dotted line) or 2 (solid line) protons, both with p$K = 7.25$. (C) difference spectra versus the oxidised enzyme of $\mathbf{P}_M$ generated at pH 9 (solid line) or pH 6 (dashed line, multiplied by 8).

Apart from changes in its magnitude, the spectrum of $\mathbf{P}_M$ was pH independent between pH 6 and 9 (Fig. 4C) and identical to that of $\mathbf{P}_H$, although at low pH (< 7.0), a redshift of the Soret peak indicative of some haem reduction was observed after several minutes of incubation, concomitant with the appearance of an EPR signal (not shown) ascribed to Cu_B [29–33]. Identical features of $\mathbf{P}_M$ and $\mathbf{P}_H$ have also been observed by resonance Raman spectroscopy [34]. A noteworthy feature of the optical spectra of $\mathbf{P}_M$, particularly at low pH, was the complete absence of any distinct 580-nm band. Mixing the mixed-valence CO-compound with oxygen at low

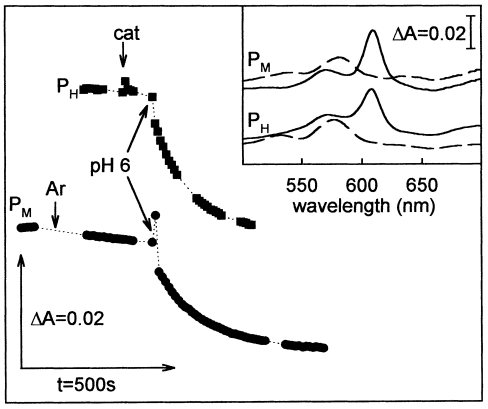

Fig. 5. Effect of pH change on $\mathbf{P}_M$ or $\mathbf{P}_H$ formed at pH 8.5. $\mathbf{P}_M$ (circles) was generated with CO/O_2 and $\mathbf{P}_H$ (squares) with 1 mM H_2O_2, both at pH 8.5, as described in the legends to Figs. 4 and 1, respectively, except that the bubbling time with CO was lowered to 15 s. $\mathbf{P}_H$ was then treated with 1000 U/ml catalase to remove excess H_2O_2, and $\mathbf{P}_M$ was purged with argon for 2 min to remove CO, as indicated. Subsequently, the pH was lowered to 6 by addition of an appropriate amount of phosphoric acid and kinetics were monitored at 608 *minus* 630 nm. The inset shows difference spectra versus the oxidised state immediately before acid addition (solid lines) and at the end of the reactions (dashed lines).

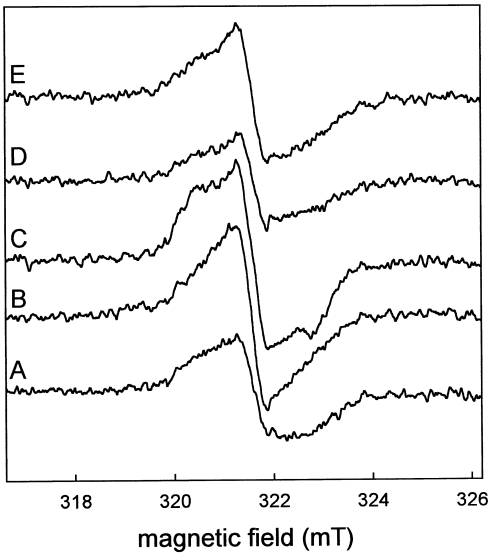

Fig. 6. EPR spectra of free radicals produced on addition of H_2O_2 to cytochrome *c* oxidase. Cytochrome *c* oxidase (35 μM) was suspended in 0.1 M MES buffer pH 6.5 (traces A–C) or 0.1 M Tricine pH 8.5 (traces D and E) containing 0.05% (w/v) lauryl maltoside and 100 U/ml superoxide dismutase. H_2O_2 additions and incubation times at room temperature were as follows: A, 50 μM H_2O_2, 1 min; B, 0.5 mM, 15 s; C, 0.5 mM 3 min; D, 50 μM, 3 min; E, 0.5 mM, 3 min. After treatment, samples were frozen in liquid nitrogen. In order to remove contributions to the spectra from oxidised Cu_A, a control spectrum has been subtracted of untreated cytochrome *c* oxidase at the same pH, recorded under identical conditions. Conditions of measurement were: temperature, 45 K; microwave power, 200 μW; microwave frequency, 9.089 G; scan speed, 5 mT min^{-1}; modulation amplitude, 0.5 mT; time constant, 0.3 s.

pH also generated only $\mathbf{P}_M$, without detectable 580-nm species. Only when $\mathbf{P}_M$ was pre-formed (at pH 8.5) and then subjected to a pH change to 6 could formation of a 580-nm compound be seen (Fig. 5). This was also the case when $\mathbf{P}_H$ was pre-formed with H_2O_2 at pH 8.5 and subjected to a pH drop to 6. Provided residual CO or H_2O_2 were removed before the pH drop, as in the experiments of Fig. 5, the observed rate constants of conversion were equivalent, consistent with the identity of $\mathbf{P}_M$ and $\mathbf{P}_H$. However, this rate constant was estimated to be 0.01 s^{-1}, which is two orders of magnitude lower than the 1–2 s^{-1} required at pH 6 for the mechanism shown in Scheme 1 of Fig. 2.

A further test of identity of $\mathbf{P}_M$ with $\mathbf{P}_H$ is a comparison of their reaction with H_2O_2 to give a 580-nm compound. In order to minimise interference of residual oxidised enzyme, the kinetics of the $\mathbf{P}_M$ reaction were studied only at pH 8.5 where the initial formation of $\mathbf{P}_M$ was close to quantitative. Measurements in the Soret region gave little absorbance change since the total concentration of ($\mathbf{P}_M$+**F**) remains constant, but real time experiments monitored at 607 nm *minus* 630 nm showed an H_2O_2 concentration-dependent decay of $\mathbf{P}_M$, with individual traces following monoexponential kinetics (not shown). A linear plot of k_{obs} versus H_2O_2 concentration yielded a bimolecular rate constant of 58 ± 3 $M^{-1}\,s^{-1}$, which is very similar to the estimated rate constant for the same reaction of $\mathbf{P}_H$ (Table 2). The spectrum, in particular the position of the Soret peak, of the 580-nm product of reaction of $\mathbf{P}_M$

Table 1
Matrix of extinction coefficients (in $mM^{-1}\,cm^{-1}$) for $\mathbf{P}_H$ and **F** relative to the oxidised enzyme used to simulate kinetic traces at the wavelength pairs 580–630 nm and 607–630 nm (derived from [8])

Wavelength pair	$\mathbf{P}_H$	**F**
580–630 nm	1.9	4.0
607–630 nm	10.4	1.9

Table 2
Rate constants for the reaction of bovine heart cytochrome *c* oxidase with H_2O_2 at pH 6.0 and 8.0

Reaction	Bovine cytochrome *c* oxidase					Cytochrome *bo* from *E. coli*[d]
	Scheme 1[a]		Scheme 2[a]			
	pH 6	pH 8	pH 6	pH 8		
$\mathbf{O} \rightarrow \mathbf{P}$ (M^{-1} s^{-1})	750 ± 100	550 ± 50	0.8 ± 0.1	400 ± 50	391[c]	1000–2000
$\mathbf{O} \rightarrow \mathbf{F}^{\bullet}$ (M^{-1} s^{-1})	–	–	450 ± 50	60 ± 10		–
$\mathbf{P} \rightarrow \mathbf{F}^{\bullet}$ (s^{-1})	1.6 ± 0.6	0.035 ± 0.01	–	–		1
$\mathbf{F}^{\bullet} \rightarrow \mathbf{P}$ (s^{-1})	0.1 ± 0.05	0.07 ± 0.01	–	–		negligible
$\mathbf{P} \rightarrow \mathbf{F}$ (M^{-1} s^{-1})	75 ± 25	45 ± 5	90 ± 20	35 ± 10	58 ± 3[a,b], 38[c]	200
$\mathbf{F}^{\bullet} \rightarrow \mathbf{F}$ (M^{-1} s^{-1})	–	–	50 ± 20	≤ 40		
$\mathbf{F} \rightarrow \mathbf{O}$ (s^{-1})	75 ± 25	6 ± 4	0.3 ± 0.2	15 ± 10		not determined

Kinetic analysis was carried out for the reactions depicted in Schemes 1 and 2 of Fig. 2. Also included are rate constants for cytochrome *bo* from *E. coli* at pH 8.0 [20] and values measured by Weng and Baker [18] for the reactions $\mathbf{O} \rightarrow \mathbf{P}_H$ and $\mathbf{P}_H \rightarrow \mathbf{F}$ (termed the decay phase at 606 nm by the authors) in the bovine enzyme (at pH 9).
[a]This work.
[b]$\mathbf{P}_M$+H_2O_2 at pH 8.5.
[c]At pH 9.0, from [18].
[d]From [20].

with H_2O_2 was indistinguishable from that of the **F** state formed via $\mathbf{P}_H$ by reaction of oxidised enzyme with millimolar H_2O_2 at the same pH, as in Fig. 1A.

3.4. H_2O_2 induced EPR signals

If $\mathbf{F}^{\bullet}$ is an oxyferryl species and is formed by reaction with only a single H_2O_2, as either scheme in Fig. 2 implies, then, as is the case for compound I in peroxidases, an electron must be provided by the protein thus forming an associated radical species. Two radical signals in oxidase samples treated with H_2O_2 have previously been observed by Fabian and Palmer [19], with linewidths of 45 and 11 G, respectively. Their ratio and amounts varied with pH and H_2O_2 concentration. However, at the time the existence of two ferryl forms, **F** and $\mathbf{F}^{\bullet}$, as derived from $\mathbf{P}_H$, was not recognised. Furthermore, the authors reported that the narrow signal was particularly intense at alkaline pH and millimolar H_2O_2, i.e. under conditions when **F** (and $\mathbf{P}_H$) rather than $\mathbf{F}^{\bullet}$ was formed, although it is $\mathbf{F}^{\bullet}$ that might most be expected to be associated with a radical. Hence, based on the kinetic parameters obtained in the optical experiments described above, EPR samples at different pH values and H_2O_2 concentrations were prepared to cover a range of conditions which yield known levels of $\mathbf{P}_H$, **F** and $\mathbf{F}^{\bullet}$.

We could reproduce, measuring at 45 K rather than 12 K [19], EPR spectra composed of two radical

Table 3
Comparison of occupancies of EPR detectable radicals and populations of the $\mathbf{P}_H$, $\mathbf{F}^{\bullet}$ and **F** states

trace in Fig. 6	Total radical occupancy	Population of		
		$\mathbf{P}_H$	$\mathbf{F}^{\bullet}$	**F**
A	0.13	≤ 0.03	0.70–0.85	0.04–0.11
B	0.20	0.07–0.10	0.75–0.85	0.07–0.10
C	0.24	≤ 0.03	0.50–0.60	0.40–0.50
D	0.10	0.55–0.65	0.10–0.20	0.10
E	0.15	≤ 0.10	≤ 0.05	0.85–0.93

Spin concentrations of the total radical signal (broad plus narrow) as shown in Fig. 6 were obtained by double integration as described in Section 2. Populations of the $\mathbf{P}_H$, $\mathbf{F}^{\bullet}$ and **F** states following incubation with H_2O_2 were calculated based on Schemes 1 or 2 of Fig. 2, and variations between the models are within the range of values given.

signals with 12 and 45-G linewidth, respectively (Fig. 6) and different power saturation behaviour. The higher temperature resulted in lower signal/noise in comparison to data in [19], but was used to ensure that quantitation against a $P700^+$ standard was done under conditions in which samples and standard were not saturated. Half saturation (at 45 K) occurred at 1.7 mW for the narrow and ≥ 3.2 mW for the broad signal. This is comparable with the previous results at 12 K [19], where the narrow signal was partially saturated even at 12.5 μW, whereas the broad signal only began to saturate above 0.2 mW.

The total spin concentration due to the two radical species did not exceed 24% of the total oxidase concentration (maximum at pH 6.5, 2 mM H_2O_2). Non-specific H_2O_2 effects could be excluded as the origin of the signals because they were not observed in samples preincubated with cyanide or formate or exposed to CO following the H_2O_2 treatment (not shown). The signals were not induced by free superoxide generated in the reduction of $\mathbf{P_H}$ and **F** by H_2O_2 [27] since superoxide dismutase was present and its absence did not lead to higher signal intensities (not shown). These control experiments demonstrated that the radicals are associated with the binuclear centre. Since the signals showed different power saturation behaviour (see above) and time dependencies (Fig. 6B,C) it can be concluded that they represent two distinct species. In agreement with previous results [19], the broad signal dominated at low H_2O_2 levels (Fig. 6A,D), whilst the narrow signal arose largely at increased H_2O_2 concentrations (Fig. 6B,C,E). However, there was no clear correlation between the levels of any intermediate, in particular $\mathbf{F^\bullet}$, as predicted from the above kinetic experiments, and the EPR signal intensities (Table 3).

4. Discussion

4.1. Multiplicity of 580- and 607-nm species

Following the report of a branched pathway for the H_2O_2 reaction of oxidised cytochrome *bo* from *E. coli* [20,35] the question arose as to whether bovine heart oxidase would react in a similar way. The results presented here demonstrate that at least two 580-nm species, **F** and $\mathbf{F^\bullet}$, can indeed be produced in cytochrome *c* oxidase, following reaction of **O** with one and two H_2O_2, respectively. Individual optical spectra of **F** and $\mathbf{F^\bullet}$ have been resolved. Previously Proshlyakov and co-workers have presented resonance Raman evidence that the 580-nm form in bovine cytochrome oxidase does not denote a single species [12]. Bands at 785/750 cm^{-1} and 355/340 cm^{-1} in the $^{16}O_2$ *minus* $^{18}O_2$ difference spectra have different pH dependencies and can, in retrospect, be assigned to **F** and $\mathbf{F^\bullet}$, respectively.

In contrast to the duplicity of 580-nm forms, the optical (this work) and resonance Raman [34] spectral characteristics of $\mathbf{P_M}$ and $\mathbf{P_H}$, as well as the similarity in their rate constants for their reaction with H_2O_2 to form **F** and for their spontaneous decay to 580-nm species at low pH, lead to the conclusion that these species are identical.

4.2. The relations between *F*, *F•* and *P*

The reaction kinetics with H_2O_2 can be modelled as described by Brittain et al. [20] where $\mathbf{F^\bullet}$ is generated by reversible unimolecular decay of $\mathbf{P_H}$ (Scheme 1 of Fig. 2), thus apparently extending the similarity in behaviour of different members of the haem-copper oxidase superfamily. Regardless of model, however, there are some quantitative differences between the kinetics of the *bo*-type [20] and bovine oxidases. This is illustrated in Table 2, where kinetic constants have been derived using the model in Scheme 1 (Fig. 2). The rate constants of the *E. coli* enzyme are higher throughout by a factor of between 2 ($\mathbf{O \rightarrow P_H}$) and 30 ($\mathbf{P_H \rightarrow F^\bullet}$), thus accounting for the observation that in the *E. coli* enzyme $\mathbf{F^\bullet}$ is quantitatively produced by stoichiometric H_2O_2 even at alkaline pH [35]. Furthermore, in the analysis based on Scheme 1 (Fig. 2), the rate constants of the bovine enzyme show a different pattern of pH dependency where a strong pH effect is required primarily for the spontaneous conversion of $\mathbf{P_H}$ to $\mathbf{F^\bullet}$. The $\mathbf{O \rightarrow P_H}$, $\mathbf{P_H \rightarrow F}$ and $\mathbf{F \rightarrow O}$ steps would only be weakly pH dependent. In contrast, in the *E. coli* enzyme, it is the H_2O_2-dependent reactions of $\mathbf{O \rightarrow P_H}$ and $\mathbf{P_H \rightarrow F}$ which respond most strongly to pH (p*K* of 8.3 and 7.7, respectively [20]).

However, whilst Scheme 1 of Fig. 2 was satisfactory to describe and simulate the kinetic data at different, fixed pH values, we have made a number of

observations which question its validity. Specifically, there are several points which indicate that the rate constant for interconversion of $\mathbf{P}_H$ and $\mathbf{F}^\bullet$ is not sufficiently rapid. First, when either $\mathbf{P}_H$ or $\mathbf{P}_M$ was pre-formed at alkaline pH and the pH was then dropped, decay to $\mathbf{F}^\bullet$ was observed (Fig. 5), but at rates that were orders of magnitude slower than the rate constant of 1–2 s^{-1} required by the mechanism of Scheme 1 (Fig. 2). Second, the extent of CO/O_2 induced formation of $\mathbf{P}_M$ was strongly pH-dependent, but the product did not contain appreciable $\mathbf{F}^\bullet$, even at low pH. This absence of $\mathbf{F}^\bullet$ means that its rate of reaction with CO (presumably, to regenerate **O**) must be much faster than its rate of formation from $\mathbf{P}_M$ and, in a separate experiment (not shown), we determined an observed rate constant for $\mathbf{F}^\bullet$ reaction with 1 mM CO at pH 6.5 to be 0.14 s^{-1}. Hence, both of these findings show that decay of $\mathbf{P}_H$ to $\mathbf{F}^\bullet$ is far slower than that required by Scheme 1 of Fig. 2, and, as a result, the model in Scheme 2 of Fig. 2 is favoured. In this model, $\mathbf{P}_H$ and $\mathbf{F}^\bullet$ are alternative initial products of the reaction with a single H_2O_2, but a direct $\mathbf{P}_H/\mathbf{F}^\bullet$ conversion is very slow (0.01 s^{-1}, Fig. 5). The pathway to $\mathbf{F}^\bullet$ may require uptake of proton(s), thus conferring the observed pH dependency of extent of $\mathbf{F}^\bullet$ formation, although the sequence of reaction of the proton and the H_2O_2 with the **O**-state cannot be determined from the present data. A preprotonated form of **O** involved in the H_2O_2 reaction at low pH must be distinct from the much slower (minutes to hours) low pH-induced transition from 'fast' to 'slow' enzyme since the pathway to becomes accessible within seconds of lowering the pH (data not shown) and because the 'slow' enzyme is unreactive towards H_2O_2. As yet, however, we have failed to detect any pH-dependent spectral changes in oxidised oxidase (other than those attributable to the fast/slow conversion) that would be consistent with multiple protonation states of the oxidised form.

Scheme 2 of Fig. 2 also offers a possible explanation of findings with cytochrome *c* oxidase from *Rhodobacter sphaeroides* where the conserved glutamic acid-286 had been replaced by a glutamine [36]. This enzyme appears to be unable to form **P** species, but can still generate a 580-nm form. In the light of the present analysis, this species seems likely to be $\mathbf{F}^\bullet$ which can still be formed in the mutant with a wild-type rate constant via the pathway of Scheme 2 since this does not involve a **P** intermediate.

We have previously reported that in the *E. coli bo*-type oxidase the CO/O_2-induced steady-state is characterised by an occupancy of 40% $\mathbf{F}^\bullet$ without any discernible $\mathbf{P}_M$ [13,35]. However, this measurement was made several minutes after oxygen addition. It appears likely in retrospect that that this system will behave qualitatively like the bovine system and that $\mathbf{P}_M$ will form first, with only very slow subsequent change to the $\mathbf{F}^\bullet$ state. In fact, the slowness of this transition seems evident from the later analysis reported in [6]. Lack of accumulation of $\mathbf{P}_M$ at steady state on long time scales presumably arises from differences in the rate of reaction with CO to regenerate the oxidised state.

4.3. Associated radical signals and structural implications

Both $\mathbf{F}^\bullet$ and **P** are formed from the oxidised state by addition of only two equivalents. However, $\mathbf{F}^\bullet$ appears to correspond spectrally to an oxyferryl form, a state requiring three equivalents compared to the oxidised state. This has already led to the suggestion of associated radical species [13,35]. Similar radicals could be associated with **P** as it has been argued on the basis of resonance Raman data that the oxygen–oxygen bond is already broken in this state [11,12,34], a condition also requiring a third redox equivalent. The additional electron could come from the porphyrin to form a π-cation radical as in compound I of horseradish peroxidase [37,38] although it has been argued on the basis of MCD results that the porphyrin ring is not oxidised in $\mathbf{F}^\bullet$ in the *bo*-type oxidase from *E. coli*. [13]. Alternatively, a protein radical may be formed, as is the case for compound I of cytochrome *c* peroxidase [39,40]. The histidine ligands of Cu_B, the covalently linked Tyr-244–His-240 pair (bovine numbering) revealed in the refined crystal structure [41], or possibly nearby tryptophans would be good candidates for an amino acid radical. The possibility of a Tyr-244 radical in **P** has variously been suggested recently [34,42,43]. It has also been suggested that the required electron might be taken from Cu_B, giving an EPR-silent Cu(III) species [13].

It has previously been reported that treatment of

bovine heart cytochrome *c* oxidase with H_2O_2 induces two EPR-detectable radical species [19]. The present study confirms that radical signals from two different species can be detected following the reaction with H_2O_2. Control experiments confirm that both are associated with the binuclear centre. However, in agreement with Fabian and Palmer's findings [19] there is no clear correlation between signal intensities and the simulated population of any of the intermediates. This may have a number of reasons, including temperature related equilibrium shifts on freezing. Spin coupling between some of the radical population and nearby metals could also reduce the intensity of the EPR signals. In addition, the signals may be the central feature of a very wide spectrum, such as that seen in the porphyrin π-cation radical of horseradish peroxidase [38], thus leading to an underestimation of the true spin concentration if only a section of the spectrum is used for quantitation.

Preliminary electron nuclear double resonance (ENDOR) studies suggest that the narrow and broad components may be assigned to a porphyrin π-cation radical and a tryptophan, respectively (Rigby, Jünemann, Rich and Heathcote, unpublished results). However, at present we are unable to correlate the level of either radical species with that of a specific intermediate. Furthermore, in a recent study of reaction of H_2O_2 with the homologous cytochrome *c* oxidase from *Paracoccus denitrificans* [21], only a single radical species, attributable to a tyrosine radical, was found. To complicate issues further, Fabian and Palmer [14] have suggested that even the 607-nm **P** form is itself initially a radical-bearing oxyferryl species, but that the radical in this case is quite rapidly re-reduced by unspecified means. Clearly, further investigations will be required before the radical state of each form can be defined reliably.

What is more certain, however, is that it is pH which is critical in determining whether **P** or $\mathbf{F}^{\bullet}$ is formed, with low pH favouring the route to $\mathbf{F}^{\bullet}$. If the protonation pattern of these states is the primary difference between them, then their extremely sluggish interconversion requires comment. It is proposed that such slowness is likely to arise from the positions of the protonation sites associated with each form, which are separated such that it is not possible to easily exchange protons between them. Further study of this phenomenon may provide insights into the protonatable residues involved.

Acknowledgements

This work was supported by grants from the Wellcome Trust (to P.R.R., ref. 049722/Z) and the Biotechnology and Biological Sciences Research Council (to P.H., ref. CO 6041). We would like to thank Prof. M. Wikström and Dr. S.E.J. Rigby for helpful discussions.

References

[1] G.T. Babcock, M. Wikström, Nature 356 (1992) 301–309.
[2] M. Wikström, Proc. Natl. Acad. Sci. USA 78 (1981) 4051–4054.
[3] M. Wikström, J.E. Morgan, J. Biol. Chem. 267 (1992) 10266–10273.
[4] J.E. Morgan, M.I. Verkhovsky, M. Wikstrom, Biochemistry 35 (1996) 12235–12240.
[5] A. Sucheta, K.E. Georgiadis, O. Einarsdóttir, Biochemistry 36 (1997) 554–565.
[6] J.E. Morgan, M.I. Verkhovsky, A. Puustinen, M. Wikström, Biochemistry 34 (1995) 15633–15637.
[7] M. Lauraeus, J.E. Morgan, M. Wikström, Biochemistry 32 (1993) 2664–2670.
[8] P.R. Rich, A.J. Moody, Cytochrome *c* oxidase, in: P. Gräber, G. Milazzo (Eds.), Bioelectrochemistry: Principles and Practice, Birkhäuser, Basle, 1997 pp. 419–456.
[9] M.I. Verkhovsky, J.E. Morgan, M. Wikström, Proc. Natl. Acad. Sci. USA 93 (1996) 12235–12239.
[10] D.A. Proshlyakov, T. Ogura, K. Shinzawa-Itoh, S. Yoshikawa, E.H. Appelman, T. Kitagawa, J. Biol. Chem. 269 (1994) 29385–29388.
[11] D.A. Proshlyakov, T. Ogura, K. Shinzawa-Itoh, S. Yoshikawa, T. Kitagawa, Biochemistry 35 (1996) 76–82.
[12] D.A. Proshlyakov, T. Ogura, K. Shinzawa-Itoh, S. Yoshikawa, T. Kitagawa, Biochemistry 35 (1996) 8580–8586.
[13] N.J. Watmough, M.R. Cheesman, C. Greenwood, A.J. Thomson, Biochem. J. 300 (1994) 469–475.
[14] M. Fabian, G. Palmer, Biochemistry 38 (1999) 6270–6275.
[15] B. Chance, C. Saronio, J.S. Leigh, J. Biol. Chem. 250 (1975) 9226–9237.
[16] P. Nicholls, G.A. Chanady, Biochim. Biophys. Acta 634 (1981) 256–265.
[17] J.M. Wrigglesworth, Biochem. J. 217 (1984) 715–719.
[18] L. Weng, G.M. Baker, Biochemistry 30 (1991) 5727–5733.
[19] M. Fabian, G. Palmer, Biochemistry 34 (1995) 13802–13810.
[20] T. Brittain, R.H. Little, C. Greenwood, N.J. Watmough, FEBS Lett. 399 (1996) 21–25.

[21] F. MacMillan, A. Kannt, J. Behr, T. Prisner, H. Michel, Biochemistry 38 (1999) 9179–9184.
[22] A.J. Moody, C.E. Cooper, P.R. Rich, Biochim. Biophys. Acta 1059 (1991) 189–207.
[23] H.U. Bergmeyer, K. Gawehn, M. Grassl, in: H.U. Bergmeyer (Ed.), Methoden der Enzymatischen Analyse, Verlag Chemie, Weinheim, 1970, p. 40.
[24] D.L. Williams-Smith, P. Heathcote, C.K. Sihra, M.C.W. Evans, Biochem. J. 170 (1978) 365–372.
[25] B.A. Barshop, R.F. Wrenn, C. Frieden, Anal. Biochem. 130 (1983) 134–145.
[26] C. Frieden, Trends Biochem. Sci. 19 (1994) 181–182.
[27] M.Y. Ksenzenko, T.V. Vygodina, V. Berka, E.K. Ruuge, A.A. Konstantinov, FEBS Lett. 297 (1992) 63–66.
[28] P. Brzezinski, B.G. Malmström, FEBS Lett. 187 (1985) 111–114.
[29] B. Reinhammar, R. Malkin, P. Jensen, B. Karlsson, L.-E. Andréasson, R. Aasa, T. Vänngård, B.G. Malmström, J. Biol. Chem. 255 (1980) 5000–5003.
[30] B. Karlsson, L.-E. Andréasson, Biochim. Biophys. Acta 635 (1981) 73–80.
[31] S.N. Witt, D.F. Blair, S.I. Chan, J. Biol. Chem. 261 (1986) 8104–8107.
[32] B. Karlsson, R. Aasa, T. Vänngård, B.G. Malmström, FEBS Lett. 131 (1981) 186–188.
[33] C. Greenwood, M.T. Wilson, M. Brunori, Biochem. J. 137 (1974) 205–215.
[34] D.A. Proshlyakov, M.A. Pressler, G.T. Babcock, Proc. Natl. Acad. Sci. USA 95 (1998) 8020–8025.
[35] A.J. Moody, P.R. Rich, Eur. J. Biochem. 226 (1994) 731–737.
[36] S. Jünemann, B. Meunier, N. Fisher, P.R. Rich, Biochemistry 38 (1999) 5248–5255.
[37] J.E. Roberts, B.M. Hoffman, R. Rutter, L.P. Hager, J. Biol. Chem. 256 (1981) 2118–2121.
[38] C.E. Schulz, P.W. Devaney, H. Winkler, P.G. Debrunner, N. Doan, R. Chiang, R. Rutter, L.P. Hager, FEBS Lett. 103 (1979) 102–105.
[39] B.M. Hoffman, J.E. Roberts, C.H. Kang, E. Margoliash, J. Biol. Chem. 256 (1981) 6556–6564.
[40] B.M. Hoffman, J.E. Roberts, T.G. Brown, C.H. Kang, E. Margoliash, Proc. Natl. Acad. Sci. USA 76 (1979) 6132–6136.
[41] S. Yoshikawa, K. Shinzawa-Itoh, R. Nakashima, R. Yaono, E. Yamashita, N. Inoue, M. Yao, M.J. Fei, C.P. Libeu, T. Mizushima, H. Yamaguchi, T. Tomizaki, T. Tsukihara, Science 280 (1998) 1723–1729.
[42] R.B. Gennis, Biochim. Biophys. Acta 1365 (1998) 241–248.
[43] C.W. Hoganson, M.A. Pressler, D.A. Proshlyakov, G.T. Babcock, Biochim. Biophys. Acta 1365 (1998) 170–174.